Engineering Structures 195 (2019) 113–124

Contents lists available at ScienceDirect

Engineering Structures

journal homepage: www.elsevier.com/locate/engstruct

Cyber-physical structural optimization using real-time hybrid simulation

Ruiyang Zhang[a], Brian M. Phillips[a,*], Pedro L. Fernández-Cabán[a], Forrest J. Masters[b]

[a] Univ. of Maryland, 1173 Martin Hall, 4298 Campus Drive, College Park, MD 20742, USA
[b] Univ. of Florida, 300 Weil Hall, 1949 Stadium Road, Gainesville, FL 32611, USA

ARTICLE INFO

Keywords:
Optimization
Real-time hybrid simulation
Cyber-physical systems
Earthquake engineering
Base isolation
Particle swarm optimization

ABSTRACT

Traditionally, structural optimization is a numerical process; candidate designs are created and evaluated through numerical simulation (e.g., finite element analysis). However, when dealing with complex structures that are difficult to model numerically, large errors could exist between the numerical model and the physical structure. In this case, the optimization is less meaningful because the optimal results are associated with the numerical model instead of the physical structure. Experiments can be included in the optimization algorithm to represent complex structures or components. However, the time and cost limitations are prohibitive when iteratively constructing and evaluating complete structural systems. Real-time hybrid simulation (RTHS) is an efficient and cost-effective experimental tool that combines numerical simulation with experimental testing to capture the total structural performance. This paper proposes a framework for real-time hybrid optimization (RTHO); RTHS is used to evaluate the performance of candidate designs within the optimization process. The framework creates a cyber-physical optimization environment using RTHS, a modern experimental technique with roots in earthquake engineering. This paper outlines the framework for RTHO with accompanying proof-of-concept studies. In a preliminary study, the base isolation design of a two-story building was optimized for seismic protection. RTHO was further validated for the optimal selection of multiple semi-active control law parameters for an MR damper installed in the isolation layer of a five-story base-isolated building. Both cases used RTHS to evaluate the candidate designs and particle swarm optimization (PSO) to drive the optimization. RTHO is well-suited to evaluate nonlinear experimental substructures, in particular those that do not undergo permanent damage such as structural control devices. Structural damage, if of interest, can be modeled through the numerical component. This paper proposes and demonstrates the integration of state-of-the-art optimization algorithms with state-of-the-art experimental methods – a cyber-physical approach to structural optimization.

1. Introduction

In the last two decades, design trends for civil infrastructure have shifted from prescriptive code procedures to performance-based methods. The structural engineers of tomorrow will be asked to produce lighter, taller, and more cost-effective designs to meet performance demands under natural and human-made hazards. Sustainable solutions that consider long-term costs and benefits will require new approaches to design and optimization. Structural optimization enables engineers to minimize user-specified objectives (e.g., material use) while ensuring strength and serviceability requirements constraints are met (e.g., requirements for drift and acceleration). Structural optimization includes size optimization, shape optimization, and topology optimization [1]. Size optimization focuses on optimizing the cross-section of the discrete structural members such as beams and columns, or thickness of continuous material such as panels and slabs. Shape optimization allows the location of nodes and connections to vary. Topology optimization uses the distribution of material and structural connectivity to find the optimal layout of the structure for a given shape.

Optimization enables engineers to produce more efficient designs in an automated, algorithmic framework. In structural engineering, systems are often nonlinear and subject to physical or design code constraints, narrowing the field of optimization to nonlinear constrained problems. In this type of optimization, engineers seek the parameter values that minimize an objective function while subject to constraints. The optimization problem must first be expressed in this basic mathematical form and then solved using an optimization algorithm of choice.

Two major categories of optimization algorithms include gradient-based and heuristic algorithms. In gradient-based algorithms, the gradient of the objective function is used to determine which design variables have the greatest influence on the objective function. The

* Corresponding author.
E-mail address: bphilli@umd.edu (B.M. Phillips).

https://doi.org/10.1016/j.engstruct.2019.05.042
Received 27 October 2017; Received in revised form 1 November 2018; Accepted 13 May 2019

gradient may be explicitly calculated or estimated by slightly changing the variables around their current value, e.g., using finite differences [2]. The gradient is used to create a subsequent design iteration that most effectively decreases (or increases, depending on the type of problem) the objective function. The major benefit of gradient-based algorithms is that they adapt at each iteration, selecting the most efficient path toward the optimum. Examples include Newton's method, conjugate gradient method, gradient descent, and subgradient method.

In contrast to gradient-based methods, heuristic methods make few or no assumptions about the nature of the problem being optimized. Common heuristic algorithms include simulated annealing (SA) [3–5], genetic algorithms (GAs) [6,7], particle swarm optimization (PSO) [8–12], and ant colony optimization (ACO) [11,13,14]. At each iteration, a set of designs are generated with some degree of randomness applied to the design variables. The development of candidate solutions is based on probabilistic rules rather than deterministic rules. Designs that are valid as defined by the constraints are then evaluated using an analysis tools such as finite element methods (FEM). Analysis results which satisfy any remaining constraints are then evaluated using the objective function. The results are synthesized and designs that performed best help inform the next generation of solutions. These methods do not guarantee that an optimal solution will be found, however they can be applied to very complex problems and without the need to calculate a gradient. Additional benefits stem from the broad search space and randomization, which can lead to non-intuitive solutions.

The quality of the optimization not only depends on the algorithm but also on the mathematical models for the structural system being optimized. In structural engineering, optimization algorithms seek the optimal configuration of a numerical model representing a physical system. Candidate designs are numerically created and evaluated at the cost of computational time. However, when studying complex structures that are difficult to model numerically, large errors could exist between the numerical model and the physical structure. In that case, the optimization is less meaningful because the results are optimal for the numerical model instead of the physical structure. Experiments can be included in the optimization framework for complex structures or components. However, it is expensive and labor intensive to iteratively create and evaluate entire structural systems in the laboratory. Real-time hybrid simulation (RTHS) provides a cost-effective alternative to investigate the optimal performance of complex structures or components, creating a cyber-physical optimization framework.

RTHS is a powerful experiment technique to evaluate the performance of structural components subjected to dynamic excitations. RTHS provides an attractive alternative to traditional shake table testing for earthquake engineering studies [15] by combining experimental testing and numerical simulation in an efficient and cost-effective framework. Structural components for which the response is well understood are modeled numerically, greatly reducing the required laboratory space and equipment. Because only the less understood, critical structural components are physically tested, they can be large or full-scale representations of the actual components, reducing size effects. In this way, even small laboratories can conduct accurate experiments of complex structures. It is a variation of hybrid simulation; the defining feature is that the experiment is executed in real time, offering the capability to test rate-dependent components, such as seismic dampers [16,17].

One of the challenges for RTHS is that it requires a fixed, small sampling in execution of each testing cycle. Moreover, unless properly compensated, time delays and time lags introduced by the experimental equipment are likely to lead to stability and accuracy problems [18]. One of the most effective approaches to mitigate the effect of time delays and time lags is through actuator control strategies designed to compensate for the modeled dynamics of the servo-hydraulic system [19,20]. In addition, the structural damping and the relative contribution of the numerical and experimental substructures to the overall structural response plays an important role in RTHS stability and accuracy [21,22]. Accurate control of the servo-hydraulic systems enables the evaluation of structures with lower inherent damping and larger relative experimental substructures.

RTHS, a cyber-physical system in itself, is proposed herein for integration into a cyber-physical optimization framework. The numerical optimization algorithm is partitioned into numerically driven optimization and the experimental evaluation of candidate designs. Experiments are then partitioned through RTHS into numerical and experimental structural components. The proposed real-time hybrid optimization (RTHO) is a promising new approach for the optimization of structures, components, or supplemental devices that are difficult to model numerically. The framework must incorporate strategies to maintain RTHS stability and accuracy in the presence of iteratively changing structural dynamics. Variable bounds must be included to avoid RTHS instabilities. Stability checks based on the RTHS partitioning can be made prior to each test, such as those reported in Maghareh et al. [21].

This paper presents the development of a cyber-physical optimization framework for structural optimization using RTHS. The framework incorporates substructure experimental testing for accurate and cost-effective evaluation of candidate designs. The framework was explored through two proof-of-concept studies. First, a linear-elastic base-isolated structure was evaluated, facilitating accurate comparisons with numerical models. Second, the control algorithm of a magnetorheological (MR) damper was optimized to demonstrate the benefits as applied to nonlinear systems for which numerical models may be inadequate.

In RTHO, because the specimen is iteratively evaluated, it should not be subject to permanent damage. RTHO is well-suited to evaluate nonlinear experimental substructures, in particular those that do not undergo permanent damage such as structural control devices. Structural damage, if of interest, can be modeled through the numerical component. Examples of recently developed structural control technologies that could be studied through RTHO include building mass dampers with semi-active control [23], tuned inertial mass electromagnetic transducers [24], and magnetorheological elastomers as seismic isolators [25].

2. Real-time hybrid optimization (RTHO)

This section presents the development of RTHO. Particle swarm optimization (PSO) is introduced as an example optimization algorithm and integrated into the RTHO framework. PSO can be replaced by other optimization algorithms based on the problem of interest.

2.1. Particle swarm optimization

PSO is inspired by the social behavior of animals such as fish schooling, insects swarming, and birds flocking [26]. It involves a number of particles, which are initialized randomly in the search space of an objective function. The group of particles is referred to as a swarm. Each particle of the swarm represents a potential solution of the optimization problem. The particles explore the search space; their positions are updated based on their current path, their own best known design, and the swarm's best known design. In each iteration, the swarm is updated using the following equations:

$$V_i^{k+1} = \omega V_i^k + c_1 r_1 (P_i^k - X_i^k) + c_2 r_2 (P_g^k - X_i^k) \quad (1)$$

$$X_i^{k+1} = X_i^k + V_i^{k+1} \quad (2)$$

where X_i and V_i represent the current position and the velocity of the i-th particle, respectively; P_i is the best previous position of the i-th particle and P_g is the best global position among all the particles in the swarm; r_1 and r_2 are two uniform random sequences generated from U (0, 1); and ω is the inertia weight used to preserve a portion of the

previous velocity of the particle [27].

First, the swarm of particles is initialized with sequence numbers and initial velocities that are randomly distributed throughout the design space. Second, the objective function values are evaluated using the design space positions. Next, the optimum particle position at the current iteration and the global optimum particle position are updated. Then, the velocity vector of each particle is updated considering the current position of the particle, the current velocity of the particle, the best position of the particle, and the best position of the swarm. The sequence number for the position of each particle is updated. Finally, the previous steps are repeated until the pre-determined number of iterations or a stopping criteria is reached.

2.2. Development of RTHO framework

The RTHO framework is created by replacing the numerical simulation (e.g., FEM) with RTHS. The objectives calculated from the measured structural responses are used to guide the particles' movements in solution searching. RTHS is conducted for each candidate design solution (particle) under each evaluation case (excitation). The performance of the candidate designs are evaluated and the results are used to populate a subsequent group of designs for evaluation. The process continues until an acceptable solution is found. The iterative framework is illustrated in Fig. 1.

The fundamental challenges of RTHS resurface in the RTHO framework. Each RTHS experiment much be stable such that the experiment can be conducted. The design variables must be properly constrained or checked before conducting RTHS to avoid instability.

Another major challenge is the creation of a cyber-physical platform with automatic updates in particle positions (experimental specimen parameters) followed by automated execution of RTHS and analysis through the optimization algorithm. The realization of RTHO requires automatic control, data exchange, and updating. A platform was developed in AutomationDesk embedded with ControlDesk, MATLAB, and Python to achieve data exchange and update in the RTHS and optimization algorithm. AutomationDesk is a powerful test automation tool for hardware-in-the-loop (HIL) testing. Testing routines can be created graphically in AutomationDesk with libraries containing many built-in functions. The automation of testing with predefined variables (i.e., a test matrix) is simple using AutomationDesk. When using variables determined online (i.e., during optimization), the programming becomes more complex. Fig. 2 shows the testing sequence created for RTHO in AutomationDesk. Numerical substructure and excitations are defined in MATLAB with the initialization of variables and particle positions. Python scripts are used as the bridge for data exchange between MATLAB and AutomationDesk. In each iteration, the particle positions are updated following Eq. (2) and used in RTHS after checking the variable boundaries to ensure the RTHS stability. RTHS is conducted using dSPACE hardware with ControlDesk software controlling the parameters, testing process, and measurements. The sequence of conducting RTHS testing through ControlDesk is created in AutomationDesk as shown in Fig. 2(b). After each test, the measurements are processed in MATLAB to evaluate the objective functions. Local best positions are updated when a better solution is found for each particle. The global best position is then updated if a local best position is a better solution than in previous iterations. RTHS continues in following iterations with updated particles' velocities and positions until reaching the maximum iteration or triggering the stopping criteria. In addition, a pause and resume algorithm is added such that the optimization can be safely interrupted as needed.

2.3. Earthquake ground motions

The framework was analyzed and verified using a group of ground motions developed previously by Somerville [28] for use in the FEMA project on steel moment-resisting frames. The group consists of 20 horizontal ground acceleration records adjusted so that their mean response spectrum matches the 1997 NEHRP design spectrum. In this study, the group of earthquakes corresponding to downtown Los Angeles was selected for seismic hazard levels corresponding to a 10% probability of exceedance in a 50-year period. These 20 earthquake records, designated as LA01-LA20, were derived from fault-parallel (FP) and fault-normal (FN) orientations of ten earthquake records.

3. Experimental setups

This section presents the experimental setup of two proof-of-concept studies for validating the proposed RTHO framework. In a preliminary study, the base isolation design of a two-story building was optimized for seismic protection. RTHO was further validated for the optimal

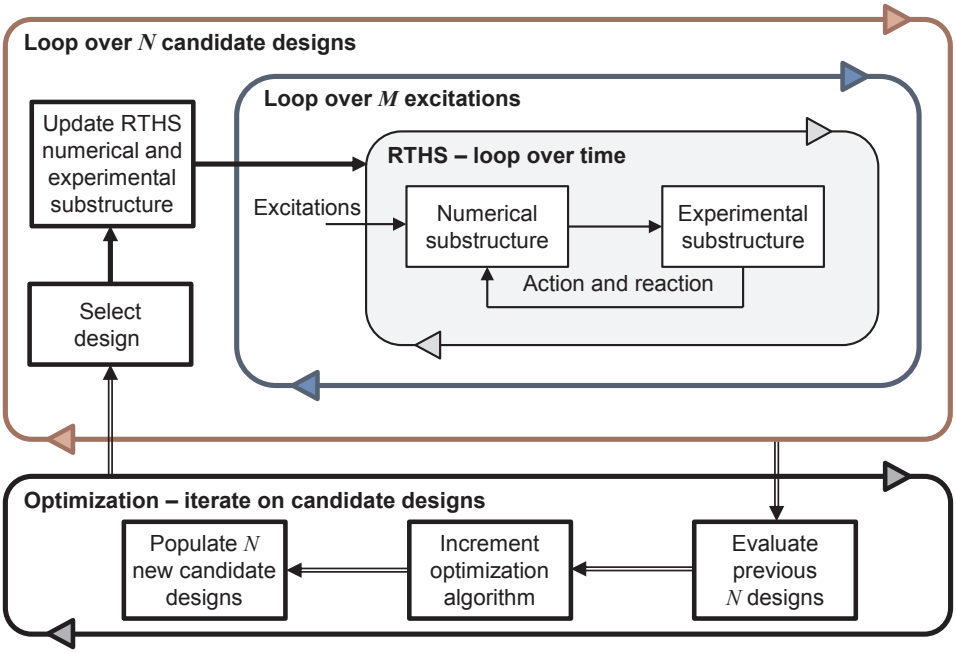

Fig. 1. Schematic of RTHO.

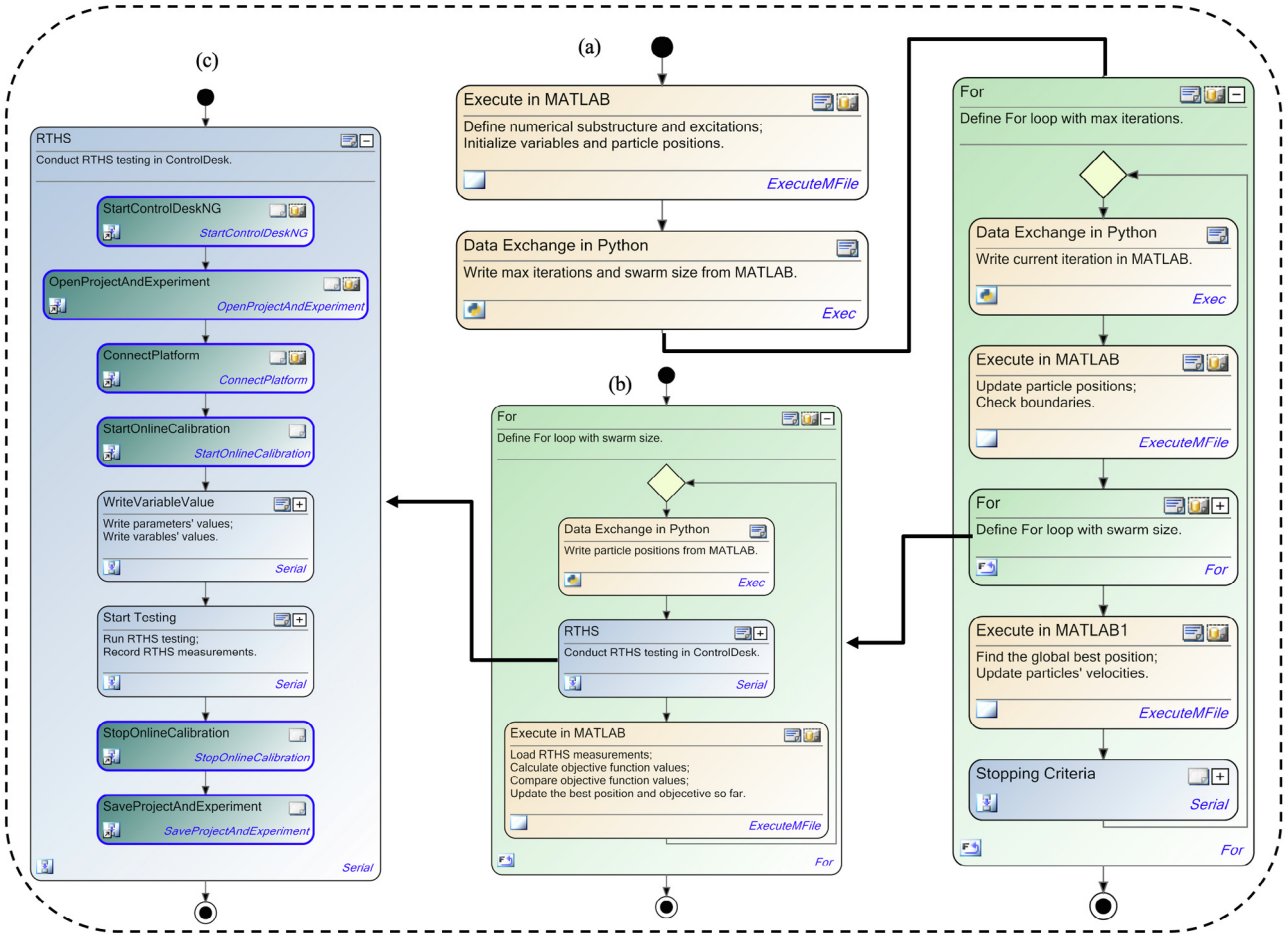

Fig. 2. Testing sequence of RTHO in AutomationDesk.

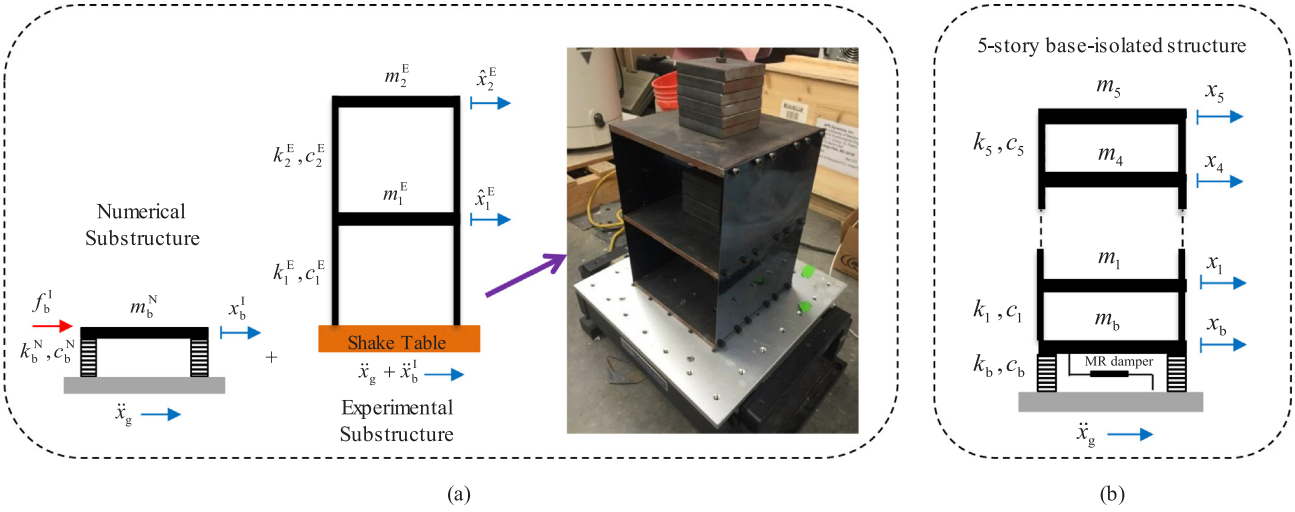

Fig. 3. (a) Two-story building specimen mounted on shake table; (b) Five-story base-isolated building with an MR damper at isolation layer.

selection of multiple semi-active control law parameters for an MR damper installed in the isolation layer of a five-story base-isolated building. This section presents the experimental setup of both the two-story and five-story building, shown in Fig. 3.

3.1. Two-story base-isolated building

The RTHO framework was verified using a small-scale experimental setup. The setup consisted of a uni-axial shake table controlling the RTHS interface between numerical and experimental substructures, a two-story steel building specimen, and a control and data acquisition system. The dynamic properties of both the 2-degree-of-freedom (DOF) experimental substructure and the 3DOF total structure are presented in this section. The specimen and equipment are located at the University of Maryland and is part of the Structural Engineering Laboratory.

3.1.1. Uni-axial shake table and sensors

The uni-axial shake table used in this study is a model APS 400 ELECTRO-SEIS manufactured by SPEKTRA. It has a 35.6 cm × 35.6 cm top plate driven by an electrodynamic vibration generator with a stroke of ±15.8 cm. The shake table has a dynamic load capacity of 445 N and it can support a payload up to 23 kg.

The control hardware for the shake table consisted of a dSPACE DS1103 Controller Board and a windows-based host PC. The controller board, working as a real-time controller, is fully programmable from the MATLAB Simulink block diagram environment. The dSPACE board performs numerical integration, provides shake table control through the proposed algorithms, and records all data. The sensors and data acquisition system included a dSPACE 16-bit high-speed multifunction data acquisition board with 8 D/A channels and 20 A/D channels, a 4-channel PCB Piezotronics signal conditioner (Model 4821C), and four PCB Piezotronics accelerometers (Model 393B04). The accelerometers have a measurement range of ±5 g, a frequency range of 0.05–750 Hz, and a sensitivity of 1000 mV/g. The accelerometers were attached on both shake table and the specimen. The overall RTHO was controlled by dSPACE's AutomationDesk.

The input-output model of the shake table is determined using a 0–10 Hz band-limited white noise voltage command to the shake table and measured acceleration of the base. A feedforward controller is created as an inverse of the identified model to compensate for the modeled dynamics of the shake table, reducing time delays and time lags for stable shake table RTHS. This approach to shake table RTHS is further discussed in Zhang et al. [22].

The reference earthquakes of Table 1 were passed through a 2-pole Butterworth high-pass filter with a cutoff frequency of 0.25 Hz to remove the low-frequency drift without altering the desired frequency content. The earthquake records were scaled down to 5% for LA15 and LA16 and 10% for all other records (relative to the magnitudes shown in Table 1) in experiments due to the stroke limitation of the small-scale shake table. All acceleration measurements in time-domain were filtered using a low-pass filter with a cutoff frequency of 20 Hz in post processing.

3.1.2. Experimental setup

A two-story steel building model was used as the experimental specimen in this study as shown in Fig. 3(a) mounted on the shake table. The floor size is 20.3 cm × 20.3 cm and the height of each story is 14.0 cm. At each floor, six steel blocks was attached as additional masses. The total mass of the first and second floors was 6.36 kg and 6.40 kg, respectively. Two spring steel sheets (SAE Grade 1095) with a thickness of 0.5 mm connected the floor plates as shown in Fig. 3. The spring steel's high yield stress ensured that the building could undergo large deformations without yielding. The bare steel structure exhibited very low inherent damping, approximately 0.95% and 0.23% for the 1st and 2nd modes, which was insufficient for stability during RTHS. The apparent damping ratios of the specimen was increased to 5% in both modes through an artificial specimen damping method proposed by the Zhang and Phillips [29].

The specimen was subjected to a 0–10 Hz band-limited white noise base excitation to determine the natural frequencies and extract the stiffness. The stiffness is determined as 2.81 kN/m for the 1st story and 4.08 kN/m for the 2nd story. The identified mass, damping, and stiffness were combined into a 2 degree-of-freedom (DOF) building model. The first and second natural frequencies of the structure were 2.2 Hz and 6.3 Hz, respectively.

The total two-story base-isolated building consisted of a numerically simulated base isolation and experimentally represented upper stories. The mass of the base was chosen as the average of the mass of the upper two stories. The stiffness of the isolation was selected as 0.61 kN/m, resulting in undamped natural frequencies of 0.85 Hz, 3.82 Hz, and 6.44 Hz. The viscous damping coefficient of base isolation was selected as the design variable for optimization.

3.2. Five-story base-isolated building with MR damper

To investigate nonlinear systems where numerical models may be inadequate, RTHO was used to optimize the semi-active control law of a large-scale MR damper. Numerical models of MR dampers are available, however their accuracy drops under semi-active conditions. For this study, the damper was considered as supplemental seismic protection for a base-isolated building. The building was five stories with one horizontal DOF per story including the base. The building was assumed to behave linear elastically because of the supplemental protection from the MR damper. The structural properties of the building can be found in Zhang and Phillips [30] and are based on a low-damping base-isolation control study in Johnson et al. [31]. For the superstructure above the isolation layer, the fundamental natural frequency is 1.85 Hz and the damping ratio in first mode is 2%. For the total structure, the fundamental natural frequency is 0.40 Hz and the damping ratio in the first mode is 4%. The MR damper was installed in the isolation layer to increase damping as shown in Fig. 3(b). The MR damper was experimentally evaluated while the rest of system was

Table 1
Earthquake index for structural optimization.

Index	Description	Magnitude	Distance	Scale Factor	PGA (g)
LA01	FN Imperial Valley, 1940, El Centro	6.9	10.0	2.01	0.46
LA02	FP Imperial Valley, 1940, El Centro	6.9	10.0	2.01	0.68
LA03	FN Imperial Valley, 1979, Array #05	6.5	4.1	1.01	0.39
LA04	FP Imperial Valley, 1979, Array #05	6.5	4.1	1.01	0.49
LA05	FN Imperial Valley, 1979, Array #06	6.5	1.2	0.84	0.30
LA06	FP Imperial Valley, 1979, Array #06	6.5	1.2	0.84	0.23
LA07	FN Landers, 1992, Barstow	7.3	36.0	3.20	0.42
LA08	FP Landers, 1992, Barstow	7.3	36.0	3.20	0.43
LA09	FN Landers, 1992, Yermo	7.3	25.0	2.17	0.52
LA10	FP Landers, 1992, Yermo	7.3	25.0	2.17	0.36
LA11	FN Loma Prieta, 1989, Gilroy	7.0	12.0	1.79	0.67
LA12	FP Loma Prieta, 1989, Gilroy	7.0	12.0	1.79	0.97
LA13	FN Northridge, 1994, Newhall	6.7	6.7	1.03	0.68
LA14	FP Northridge, 1994, Newhall	6.7	6.7	1.03	0.66
LA15	FN Northridge, 1994, Rinaldi RS	6.7	7.5	0.79	0.53
LA16	FP Northridge, 1994, Rinaldi RS	6.7	7.5	0.79	0.58
LA17	FN Northridge, 1994, Sylmar	6.7	6.4	0.99	0.57
LA18	FP Northridge, 1994, Sylmar	6.7	6.4	0.99	0.82
LA19	FN North Palm Springs, 1986	6.0	6.7	2.97	1.02
LA20	FP North Palm Springs, 1986	6.0	6.7	2.97	0.99

modeled numerically through RTHS. In the RTHS loop, the numerically evaluated base DOF displacement was input to the physical MR damper using a servo-hydraulic actuator. The restoring force measured by the actuator was then returned to the numerical model. This loop of action and reaction continued for the duration of each RTHS experiment.

3.2.1. Semi-active control law

The semi-active control law for the MR damper was based on a causal model for rate-independent linear damping (RILD). RILD provides direct control over displacement, a desirable feature for low-frequency structures such as base-isolated structures. When low-frequency structures are subjected to high-frequency ground motions, RILD produces similar reduction in response displacements and velocities when compared to viscous damping; however, the damping forces and floor accelerations are substantially smaller. In RILD, the restoring force is proportional to displacement but advanced in phase $\pi/2$ rad, a non-causality that has limited its practical applications. To realize the benefits of direct displacement control for low-frequency structures, a causal realization of RILD was proposed in Keivan et al. (2017). The causal model uses a first-order all-pass filter to approximate the desired RILD force. This model, shown in Eq. (3), was taken as the primary semi-active control law. The isolation layer displacement was input to the model and the output was taken as the desired force in the MR damper. A secondary semi-active controller (clipped-optimal control; Dyke et al. [32]) was then used to minimize tracking error between desired and measured MR damper forces.

$$F_{\mathrm{D,causal}}(\omega) = k\eta\left(\frac{i\omega - \omega_f}{i\omega + \omega_f}\right) \tag{3}$$

Two parameters are present in the primary semi-active control law: the loss factor η and radial frequency ω_f. The loss factor η affects the RILD force magnitude and is present in both causal and non-causal models. The radial frequency ω_f is only present in the causal model (Eq. (3)) and adjusts the skew of the force-displacement hysteresis. If ω_f exactly matches the response frequency across the isolation layer, then the hysteresis will show zero skew, creating a perfect match with non-causal RILD. The optimal values for these parameters depend on the design objective as well as the dynamics of the structure and the magnitude and frequency content of the ground motions.

3.2.2. Experimental setup

Fig. 4 shows the testing setup of this structure. The specimen is a second-generation 200-kN MR damper manufactured by Lord Corporation. The unique properties of MR dampers are derived from the internal MR fluid. When a magnetic field is applied, the fluid changes from a linear viscous fluid to a semi-solid with controllable yield strength. The actuator and MR damper were mounted on steel angle plates placed on top of an I-beam that was secured to the strong floor using tie-downs. The actuator and MR damper were connected through a connection plate with a large threaded rod and four high strength bolts. A 250-kN MTS servo-hydraulic controlled actuator was used to provide the boundary interaction (e.g., displacement and force in real time) from numerical substructure. Displacement was measured using a linear variable differential transformer (LVDT) and force was measured using a load cell. A model-based actuator controller was developed to reduce actuator time delay and time lag [33].

4. Results

4.1. Two-story base-isolated building

This section presents the performance of RTHO for the two-story base-isolated building introduced in Section 3.1. PSO was used for optimal solution searching with the objective of minimizing maximum structural absolute acceleration across all ground motions considered and the constraint of maintaining base drifts under 2 cm (model scale). The damping coefficient c_b of base isolation was taken as the design variable. To ensure the RTHS stability, c_b was restrained with a lower limit of 4.55 Ns/m, which gives a 2% damping ratio in 1st mode. An upper limit of 201.73 Ns/m was used to ensure that the damping ratio of fundamental mode never exceed 100%. For PSO, a swarm with five particles and a maximum iteration of 50 was considered. The inertia weight in Eq. (1) was selected as 1.0 and acceleration coefficients were each selected as 2.0. The study first looks at optimization under a single earthquake excitation. Then, it follows with optimization under several earthquakes. Lastly, the optimization under all 20 design earthquakes was conducted. To demonstrate the performance of RTHO, results are compared to PSO using numerical simulation (FEM) to evaluate candidate solutions. Two cases are listed below.

1. Optimization of the base-isolated building in numerical simulation (OPT-SIM); and
2. Cyber-physical optimization of the base-isolated building, where the upper two stories are physically tested and the base isolation is numerically modeled (RTHO).

Overall agreement between RTHO and OPT-SIM was expected; the linear-elastic structure is a proof-of-concept. Table 2 summarizes all results with details given in the following subsections. Minimum peak absolute accelerations match well for all earthquake scenarios. Discrepancies between RTHO and OPT-SIM appear most clearly in the damping value that achieves the minimum peak acceleration. This difference can be attributed to the relatively flat solution space around the minimum peak acceleration where large changes in c_b produce small changes in the minimum peak acceleration. This makes the optimal c_b sensitive to errors in numerically modeling the specimen and experimental error including measurement noise and shake table control.

4.1.1. Structural optimization using RTHO under a single earthquake

First, the optimal design of the base-isolated building was investigated when subjected to LA02. The objective was to minimize the maximum structural absolute acceleration for all DOF i under LA02 as

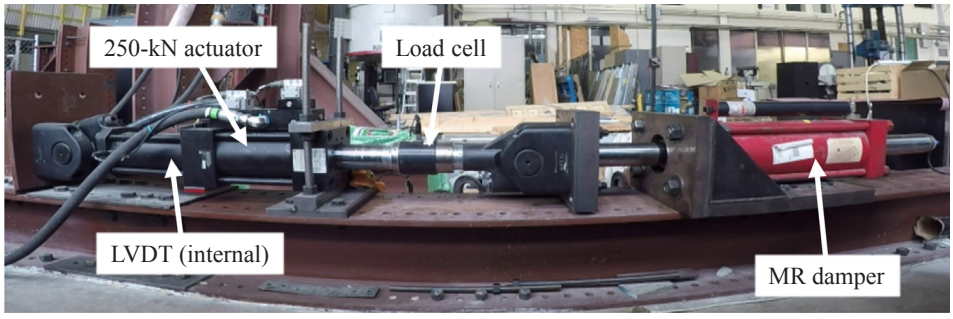

Fig. 4. Testing setup of large-scale MR damper for RTHS testing.

Table 2
Comparison summary of RTHO and OPT-SIM results.

Criteria	Single earthquake		Multiple earthquakes		Suite of earthquakes	
	RTHO	OPT-SIM	RTHO	OPT-SIM	RTHO	OPT-SIM
Optimal c_b (Ns/m)	48.0	61.4	43.8	50.4	77.2	102
Minimum peak acceleration (m/s^2)	0.4661	0.4435	0.4879	0.4810	0.7074	0.6763
Percent difference in acceleration (relative to OPT-SIM)	5.10%		1.43%		4.60%	

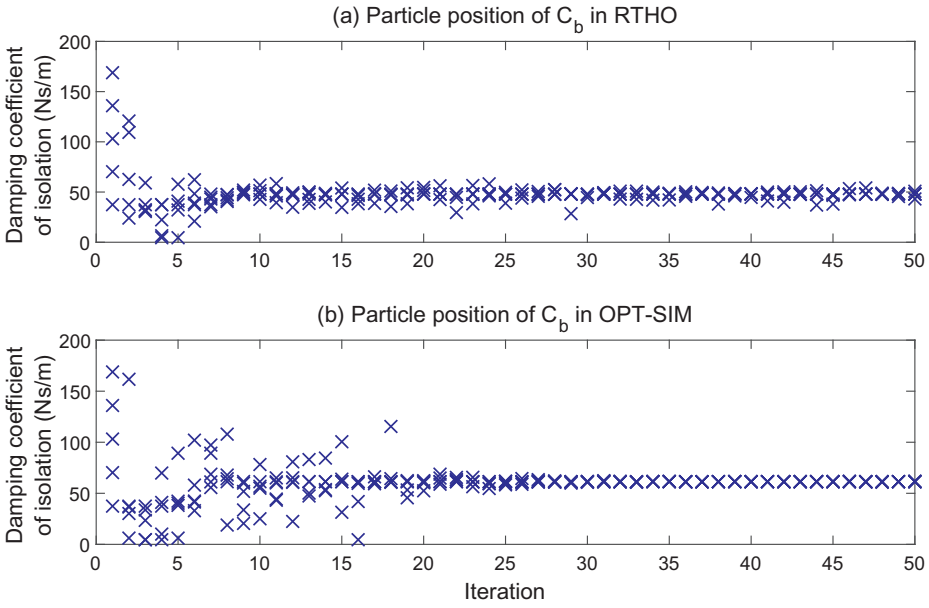

Fig. 5. Particle positions in optimization in (a) RTHO; (b) OPT-SIM.

Eq. (4) through optimization of c_b.

$$\min\left[\max_{LA02}\left\{\max_{t,i}\ |\ddot{x}^{i}_{abs}(t)|\right\}\right] \tag{4}$$

The particle positions over iterations from optimization in RTHS and SIM are shown in Fig. 5(a) and (b), respectively. Fig. 6(a) and (b) show the iteration history of the objective function values for optimization in RTHS and SIM respectively. The convergence of particle position and objective function can be clearly observed from both figures. The optimal viscous damping coefficient of the isolation layer is found to be 47.98 Ns/m, achieving the smallest maximum absolute acceleration of 0.4661 m/s^2. The damping ratio is around 19.0% in the fundamental mode. The optimal solution obtained using the RTHO framework is comparable to the optimal solution from OPT-SIM, which is 61.41 Ns/m minimizing the maximum structural acceleration to 0.4435 m/s^2. Good agreement is observed between RTHO and OPT-SIM optimal acceleration, as shown in Table 2. Fig. 7 shows the structural responses with the optimal damping of base isolation. Results match well between the optimal design using both RTHO and OPT-SIM. The base drift is within the constraint of 0.02 m.

4.1.2. Structural optimization using RTHO under a suite of design earthquakes

Seismic design of building structures often considers a suite of earthquakes with the response spectrum matching the design spectrum (e.g., LA01-LA20). In this section, the viscous damping coefficient of the isolation layer was optimized to improve structural responses

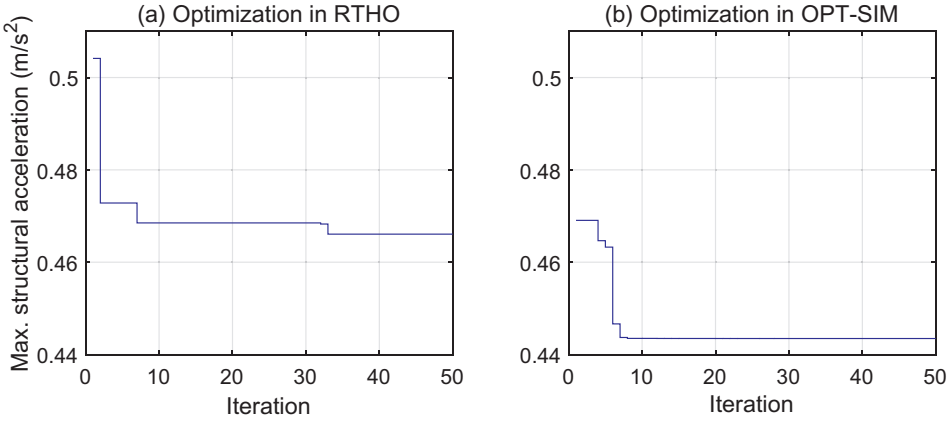

Fig. 6. Iteration history of objective functions for optimization in (a) RTHO; (b) OPT-SIM.

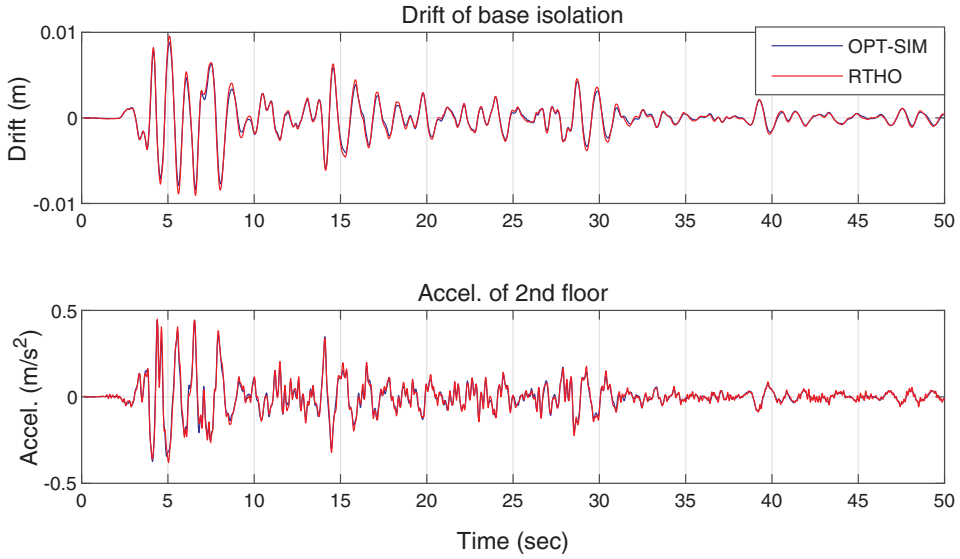

Fig. 7. Time history analysis of the optimal design from RTHO and OPT-SIM.

considering all design earthquakes. The objective, therefore, was to minimize the maximum structural absolute acceleration under the worst earthquake excitation as Eq. (6).

$$\text{minimize} \quad \max_{LA01}^{LA20} |\ddot{x}_{abs}| \tag{6}$$

It is time-consuming and inefficient to evaluate all 20 earthquakes during optimization. To achieve optimal design more quickly, a preliminary test matrix was create to determine the general relationship between isolation layer damping and the maximum structural acceleration under all 20 earthquakes. Five discrete damping coefficients uniformly distributed between [4.55, 201.7] Ns/m were selected as 37.41, 70.28, 103.1, 136.0, and 168.9 Ns/m. The bar plot in Fig. 8 shows the maximum structural accelerations at the five damping coefficients under all design earthquakes. Note that is not an optimization run, rather a test matrix used to narrow down the earthquakes considered. For each damping coefficient, the worst earthquake resulting in the maximum acceleration was found. To be more conservative, the worst two earthquakes for each damping coefficient were selected as the dominant earthquake candidates. From Fig. 8, it can be clearly seen that the maximum acceleration happens under the worst two earthquakes {LA20, LA14}, {LA18, LA20}, {LA18, LA19}, {LA19, LA18}, and {LA19, LA18} for the five damping coefficients respectively. A consistent conclusion was obtained for test matrices created using RTHS and numerical simulation (FEM/SIM) in Fig. 8. Therefore, earthquakes LA14, LA18, LA19, and LA20 were determined as the dominant earthquake candidates for structural optimization. This approach works well when the number of design variable is small, e.g., in this case the only design variable is the supplemental viscous damping in the isolation layer. More efficient algorithms will be developed for many design variables in future studies (e.g., multi-interval PSO in Zhang et al. [34]).

Based on the governing earthquakes selected, optimization was run for both RTHO and OPT-SIM cases. Fig. 9 shows the particle positions of damping coefficients during optimization in RTHS and SIM. The optimal damping coefficient is found as 77.20 Ns/m in RTHO with a damping ratio of 30.7% in 1st mode, compared to the optimal damping coefficient in OPT-SIM as 101.9 Ns/m. The iteration history of objectives is shown in Fig. 10(a) and (b) for optimization in RTHO and OPT-SIM respectively. The achieved optimal objective is 0.7074 m/s^2 in RTHS and 0.6763 m/s^2 in SIM. Good agreement is observed between RTHO and OPT-SIM in optimizing the structural performance subjected to all 20 designed earthquakes as shown in Table 2. Fig. 11 shows the time history of the base drift and acceleration of top floor under the dominant earthquake LA20 (i.e., the worst earthquake for the optimal design). Time history responses match well between RTHO and OPT-SIM. Note that after obtaining the optimal designs for both RTHO and OPT-SIM, the optimal designs were evaluated under all 20 earthquakes.

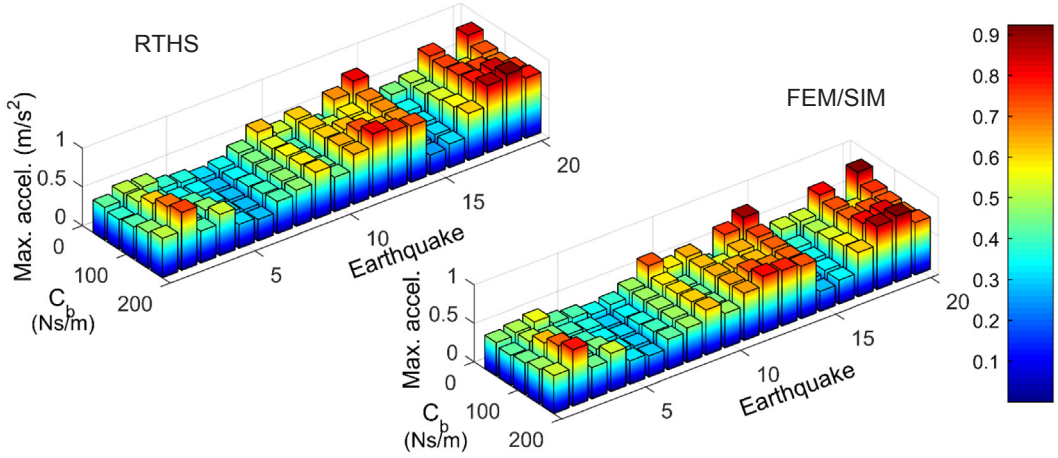

Fig. 8. Relationship of damping ratio and earthquakes on structural acceleration.

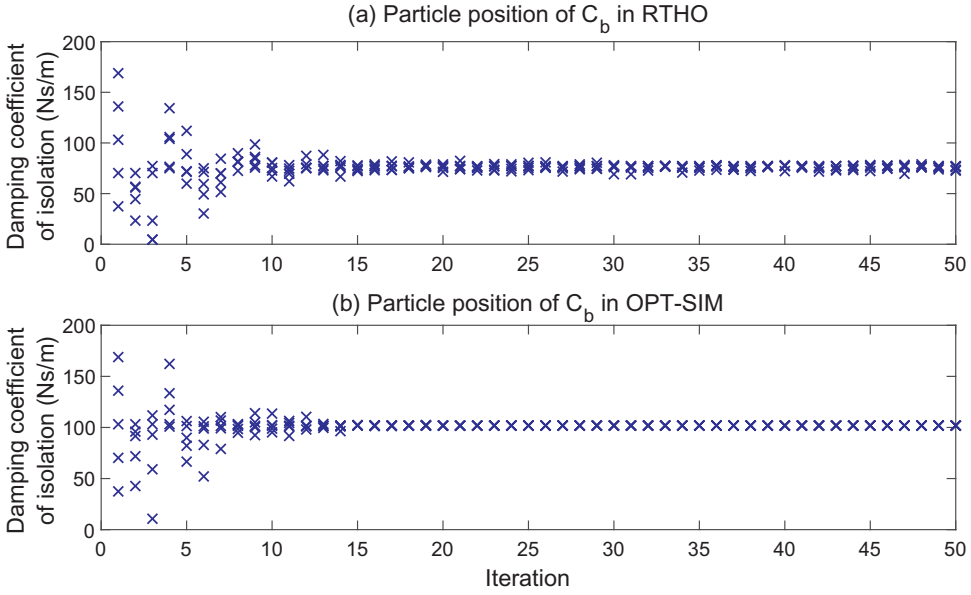

Fig. 9. Particle positions in optimization in (a) RTHO; (b) OPT-SIM.

This comprehensive evaluation confirmed that the selected earthquakes did govern for the optimal solution.

4.2. Five-story base-isolated building with MR damper

The optimal seismic design of the five-story base-isolated building with supplemental control, introduced in Section 3.2, was conducted using the proposed RTHO framework. PSO was used as the search algorithm in this study with a swarm of five particles and a maximum iteration of 50. Each particle has two DOF, i.e., the two control law design parameters η and ω_f. The objective was selected to minimize the maximum absolute structural accelerations as given in Eq. (3). Additionally, the isolation drift was constrained under 10 cm for experimental safety and practical design limitations. The design earthquake was taken as LA02 with a magnitude scaling of 20%. As in the previous study, additional earthquakes can be included as required.

Fig. 12 shows the particle positions over iterations for the optimization in RTHS. The optimal positions of η and ω_f are found as 0.2720 and 4.2327 rad/s, respectively. The objective function history is shown in Fig. 13 with a minimum maximum absolute acceleration of 0.4637 m/s^2 achieved. The convergence of multiple variables and objective can be clearly seen from both figures. Fig. 14 shows the actuator tracking performance using the feedforward controller for the final optimal design. A near perfect match is observed between desired and measured responses, showing that the boundary conditions between substructures in RTHS was achieved. The drift of base isolation is maintained within the 10 cm limit. Fig. 15 shows the MR damper control performance with optimal control of η and ω_f as 0.2720 and 4.2327 rad/s. The hysteresis of the MR damper is shown in Fig. 16. The MR damper's clipped-optimal controller is able to track the desired forces from Eq. (3) as observed between desired and measured behavior. The hysteresis of the optimal design has a large enclosed area to increase damping and a slight negative skew to reduce accelerations.

5. Conclusions and recommendations

This study presents a new approach for conducting structural optimization. The proposed RTHO framework is a cyber-physical optimization environment; optimization is numerically driven while the evaluation of candidate designs is conducted experimentally using RTHS. RTHS offers an efficient and cost-effective test method through the substructuring of dynamic systems into numerical and experimental components, another example of a cyber-physical system. The development of RTHO is discussed in detail and built around PSO, a popular heuristic search algorithm. PSO offers many benefits including broad search of the solution space; however, RTHO can easily be adapted to any optimization algorithm.

RTHO was demonstrated to be effective in both linear elastic and

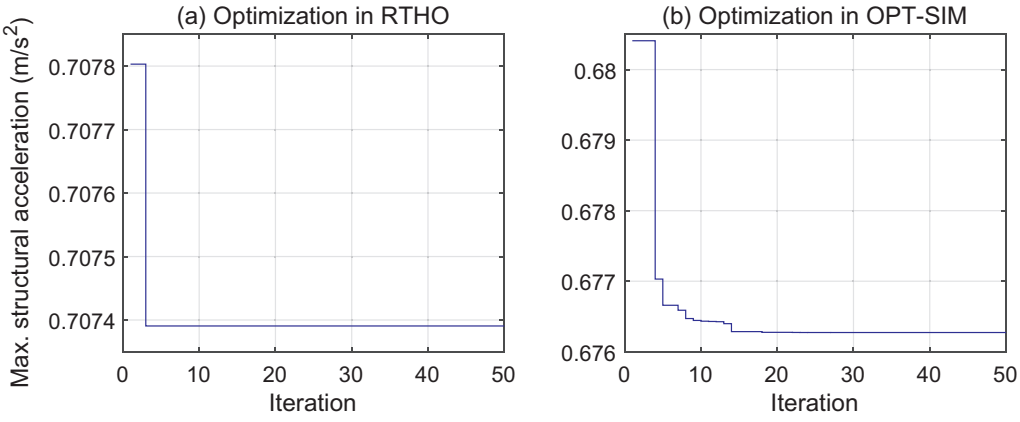

Fig. 10. Iteration history of objective functions for optimization in (a) RTHO; (b) OPT-SIM.

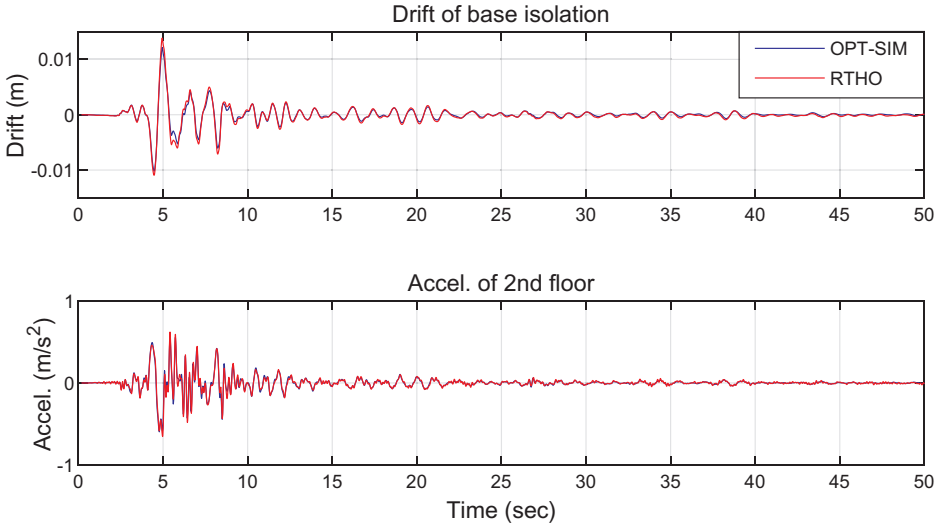

Fig. 11. Time history analysis of the optimal design from RTHO and OPT-SIM under LA20.

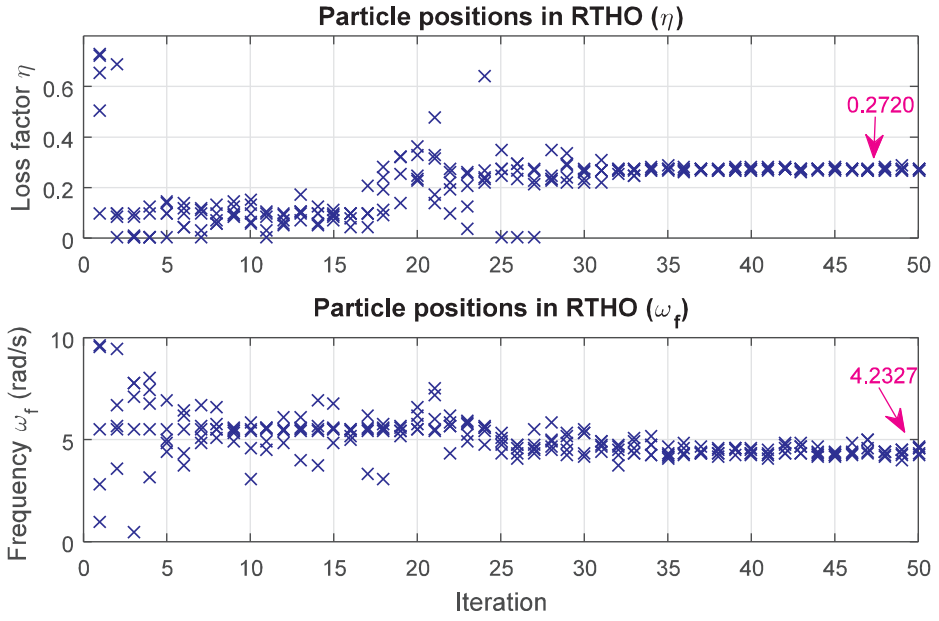

Fig. 12. Particle positions in RTHO.

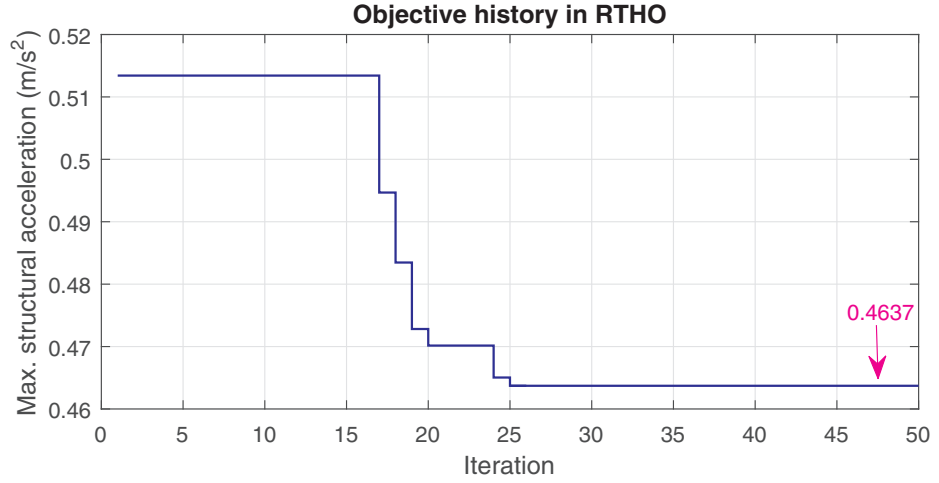

Fig. 13. Iteration history of objective function in RTHO.

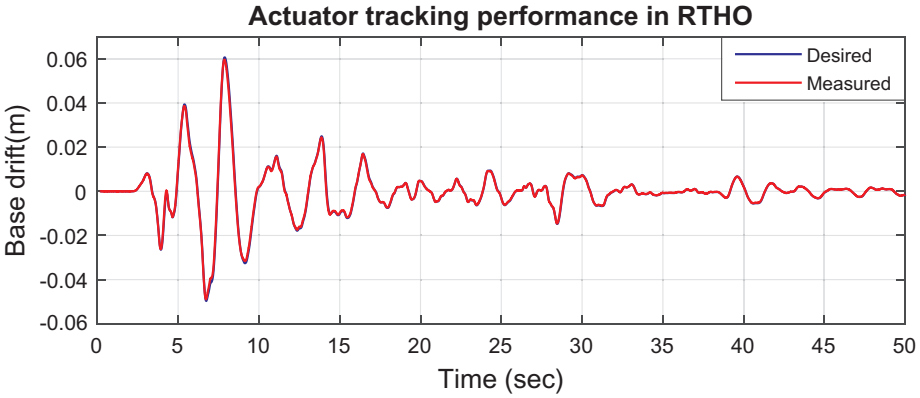

Fig. 14. Time history of actuator (base drift) for the optimal design under LA02.

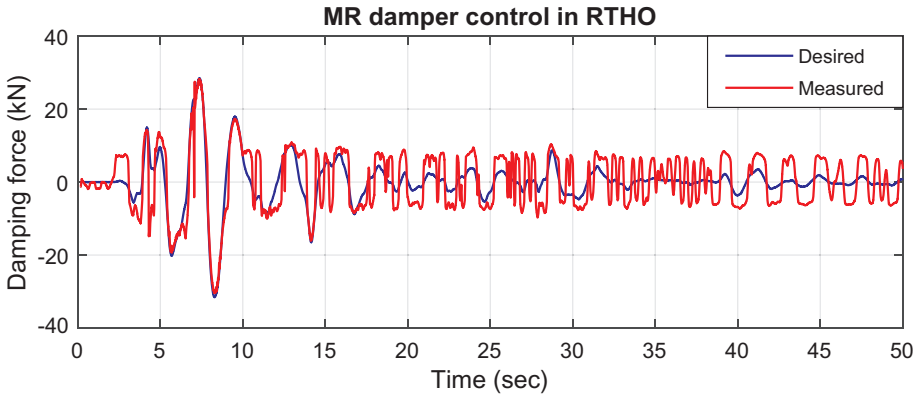

Fig. 15. Time history of damping force for the optimal design under LA02.

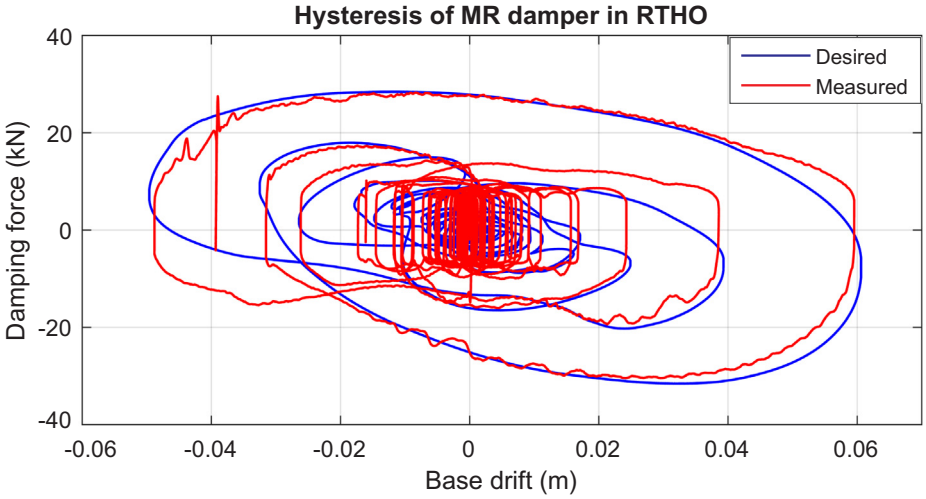

Fig. 16. Hysteresis of MR damper for the optimal design under LA02.

nonlinear proof-of-concept studies. Through the RTHO, the base isolation design of a linear elastic structure was optimized for the seismic protection of a two-story building. The optimal design against single and multiple earthquakes was conducted to show the versatility for inclusion in performance-based design. The results using RTHO were compared with numerical optimization. Overall good agreement is observed between RTHO and numerical optimization for this simple structure, building confidence in applying RTHO to study complex systems that are difficult to model numerically. To show the benefits of RTHO when numerical models may be inadequate, a five-story base-isolated building with a nonlinear MR damper at the isolation layer was investigated. The control law of a physically modeled MR damper as optimized to mitigate structural acceleration against seismic loads. RTHO quickly converged for the nonlinear and multi-variate optimization problem. The hysteresis for the optimal solution looks as expected, with a large enclosed area to increase damping and a slight negative skew to reduce accelerations.

The RTHO approach has many potential applications in civil engineering across a variety of hazards. In particular, the approach can be applied to structural control problems when the specimen is designed not to experience permanent damage and can be iteratively evaluated. Additionally, in wind engineering many specimens are designed not to

experience damage and are suited for repeated experiments. RTHS, a cyber-physical system in itself, is well suited for integration into a cyber-physical optimization environment.

Acknowledgements

The authors would like to acknowledge the National Science Foundation (NSF), USA Grant No. 1636039 (PI: Brian Phillips, Co-PI: Forrest Masters). Developments in cyber-physical optimization for wind engineering through this grant inspired the discussions that led to this research paper. Any opinions, findings, and conclusions or recommendations expressed in this material are those of the authors and do not necessarily reflect the views of NSF. The authors would also like to thank Richard E. Christenson for the use of the 200-kN MR damper.

References

[1] Rozvany GI. A critical review of established methods of structural topology optimization. Struct Multidiscip Optim 2009;37(3):217–37.
[2] Azadivar F. A tutorial on simulation optimization. In: Proceedings of the 24th conference on Winter simulation. ACM. p. 198–204.
[3] Kirkpatrick S, Gelatt CD, Vecchi MP. Optimization by simulated annealing. Science 1983;220(4598):671–80.
[4] Juan H, Yu SF, Lee BY. The optimal cutting-parameter selection of production cost in HSM for SKD61 tool steels. Int J Mach Tools Manuf 2003;43(7):679–86.
[5] Wang ZG, Rahman M, Wong YS, Sun J. Optimization of multi-pass milling using parallel genetic algorithm and parallel genetic simulated annealing. Int J Mach Tools Manuf 2005;45(15):1726–34.
[6] Davis L. Handbook of genetic algorithms; 1991.
[7] Li H, Li X. Modelling and simulation of chatter in milling using a predictive force model. Int J Mach Tools Manuf 2000;40(14):2047–71.
[8] Eberhart R, Kennedy J. A new optimizer using particle swarm theory. MHS'95. Proceedings of the sixth international symposium on micro machine and human science. Ieee; 1995. p. 39–43.
[9] Tandon V, El-Mounayri H, Kishawy H. NC end milling optimization using evolutionary computation. Int J Mach Tools Manuf 2002;42(5):595–605.
[10] Kurdi MH, Schmitz TL, Haftka RT, Mann BP. Simultaneous optimization of removal rate and part accuracy in high-speed milling. In ASME 2004 International Mechanical Engineering Congress and Exposition, pp. 1001–1009. American Society of Mechanical Engineers.
[11] Baskar N, Asokan P, Prabhaharan G, Saravanan R. Optimization of machining parameters for milling operations using non-conventional methods. Int J Adv Manufact Technol 2005;25(11):1078–88.
[12] Kurdi MH. Robust multicriteria optimization of surface location error and material removal rate in high-speed milling under uncertainty. Doctoral dissertation. University of Florida; 2005.
[13] Dorigo M, Di Caro G. Ant colony optimization: a new meta-heuristic. Proceedings of the 1999 congress on evolutionary computation-CEC99 (Cat. No. 99TH8406), vol. 2. IEEE; 1999. p. 1470–7.
[14] Dorigo M, Birattari M. Ant colony optimization. Springer, US; 2010.
[15] Nakashima M, Kato H, Takaoka E. Development of real-time pseudo dynamic testing. Earthq Eng Struct Dyn 1992;21(1):79–92.
[16] Christensen RE, Lin Y, Emmons A, Bass BJ. Large-scale experimental verification of semi-active control through real-time hybrid simulation. J Struct Eng 2008;134(4):522–34.
[17] Carrion JE, Spencer Jr. BF, Phillips BM. Real-time hybrid simulation for structural control performance assessment. Earthq Eng Eng Vibrat 2009;8(4):481–92.
[18] Horiuchi T, Nakagawa M, Sugano M, Konno T. Development of a real-time hybrid experimental system with actuator delay compensation. In: Proceedings of the 11th World Conf. Earthquake Engineering, Paper No. 660.
[19] Carrion JE, Spencer Jr BF. Model-based strategies for real-time hybrid testing. Newmark Structural Engineering Laboratory Report Series, University of Illinois at Urbana-Champaign, Urbana, IL, No. 6; 2007.
[20] Phillips BM, Spencer Jr BF. Model-based feedforward-feedback actuator control for real-time hybrid simulation. J Struct Eng 2012;139(7):1205–14.
[21] Maghareh A, Dyke SJ, Prakash A. Establishing a predictive performance indicator for real-time hybrid simulation. Earthq Eng Struct Dyn 2014;43(15):2299–318.
[22] Zhang R, Lauenstein PV, Phillips BM. Real-time hybrid simulation of a shear building with a uni-axial shake table. Eng Struct 2016;119:217–29.
[23] Liu YF, Lin TK, Chang KC. Analytical and experimental studies on building mass damper system with semi-active control device. Struct Control Health Monit 2018.
[24] Asai T, Araki Y, Ikago K. Structural control with tuned inertial mass electromagnetic transducers. Struct Control Health Monit 2018;25(2).
[25] Nguyen XB, Komatsuzaki T, Iwata Y, Asanuma H. Modeling and semi-active fuzzy control of magnetorheological elastomer-based isolator for seismic response reduction. Mech Syst Sig Process 2018;101:449–66.
[26] Kennedy J, Kennedy JF, Eberhart RC, Shi Y. Swarm intelligence. Morgan Kaufmann; 2001.
[27] Shi Y, Eberhart R. A modified particle swarm optimizer. In: Evolutionary Computation Proceedings, 1998. IEEE World Congress on Computational Intelligence. The 1998 IEEE International Conference on, pp. 69–73. IEEE; 1998.
[28] Somerville P. Development of ground motion time histories for Phase 2 of the FEAM/SAC steel project. SAC Background document SAC/BD-91/04, SAC joint venture, Sacramento, California.
[29] Zhang R, Phillips BM. Artificial specimen damping for substructure real-time hybrid simulation. J Eng Mech 2017;143(8):04017052.
[30] Zhang R, Phillips BM. Performance and protection of base-isolated structures under blast loading. J Eng Mech 2015;142(1):04015063.
[31] Johnson EA, Ramallo J, Spencer BF Jr, Sain MK. Intelligent base isolation systems. In: Proceedings of the 2nd World Conference on Structural Control, IASCM, Japan, p. 367–76.
[32] Dyke SJ, Spencer Jr. BF, Sain MK, Carlson JD. Modeling and control of magnetorheological dampers for seismic response reduction. Smart Mater Struct 1996;5(5):565–75.
[33] Phillips BM, Takada S, Spencer BF, Fujino Y. Feedforward actuator controller development using the backward-difference method for real-time hybrid simulation. Smart Struct Syst 2014;14(6):1081–103.
[34] Zhang R, Phillips BM. Cyber-physical approach to the optimization of semiactive structural control under multiple earthquake ground motions. Comput-Aided Civ Inf 2019.